Selecting algorithms, sensors, and linear bases for optimum spectral recovery of skylight

Miguel A. López-Álvarez, Javier Hernández-Andrés, Eva M. Valero, and Javier Romero

Departamento de Óptica, Facultad de Ciencias, Universidad de Granada, 18071 Granada, Spain

In a previous work [Appl. Opt. **44**, 5688 (2005)] we found the optimum sensors for a planned multispectral system for measuring skylight in the presence of noise by adapting a linear spectral recovery algorithm proposed by Maloney and Wandell [J. Opt. Soc. Am. A **3**, 29 (1986)]. Here we continue along these lines by simulating the responses of three to five Gaussian sensors and recovering spectral information from noise-affected sensor data by trying out four different estimation algorithms, three different sizes for the training set of spectra, and various linear bases. We attempt to find the optimum combination of sensors, recovery method, linear basis, and matrix size to recover the best skylight spectral power distributions from colorimetric and spectral (in the visible range) points of view. We show how all these parameters play an important role in the practical design of a real multispectral system and how to obtain several relevant conclusions from simulating the behavior of sensors in the presence of noise. © 2007 Optical Society of America

OCIS codes: 150.2950, 280.0280, 040.0040.

1. INTRODUCTION

Multispectral imaging systems and techniques have become powerful tools for the rapid measurement of high-spatial-resolution spectral images. They allow us to recover the spectral radiance of an illuminant, the reflectance of an object, or the combined color signal by using data from the responses of a few sensors, typically those in a CCD digital camera. In this paper we focus on skylight as an important natural illuminant from the spectral curves of which we can extract information about climate parameters such as optical depth or the Angstrom exponent.[1] These spectral power distribution curves (SPDs) are normally measured with spectroradiometers, which are complex and expensive instruments that provide only one spectrum per measurement, whereas a multispectral system such as the one simulated here will provide one accurate spectrum at each pixel of the entire image. Multispectral imaging systems,[2] therefore, are increasingly replacing classical spectroradiometers in the task of measuring SPDs owing to the substantial improvements they offer in spatial resolution, portability, and speed compared with other spectral instruments.

Faced with the task of obtaining accurate spectral measurements from a multispectral system, we must select the algorithm to recover suitable spectral curves from sensor responses, estimate and try to reduce the influence of the noise present in the system, and choose the optimum sensors or filters for the task for which this multispectral system has been designed. It is possible to take into account all these factors in a step prior to the development of the multispectral system. Computers allow us to simulate the spectral sensitivity of sensors and their response to spectral information, to add simulated noise, and to try to recover mathematically the SPD curves from this noise-influenced sensor data. If these computational models simulate the real physical phenomena accurately

enough, the information provided by them will help us to build an accurate multispectral system.

In this work we deal with all the possible factors that should be taken into account when studying the behavior of a practical multispectral system: the spectral sensitivity of its sensors, the number and type of sensors, the estimation method and linear basis chosen, the number and quality of training spectra, and the noise that always affects any electronic device. To include all these factors in an exhaustive search is a highly demanding computational task. Our alternative approach greatly reduces computing time by using a simulated annealing algorithm[3] that minimizes one cost function. To this end, in Section 3 we use a previously proposed[4] single-cost function that evaluates the quality of our recovered skylight spectra. This is known as the colorimetric and spectral combined metric (CSCM) function, which has proved to be a good metric for evaluating spectral and colorimetric differences between skylight spectra.[5]

As far as the spectral estimation method is concerned, it must be clear from the outset that extracting spectral information in the visible range from the responses of a few sensors is an under-dimensioned mathematical problem because the projection of the skylight spectra in the sensor-response space leads to a substantial loss of information. Various mathematical algorithms exist that allow us to estimate spectral information from sensor responses. These methods are commonly based on *a priori* knowledge of the kind of spectra we want to recover. For example, performing a principal component analysis[2,6–8] (PCA) or, more recently, nonnegative matrix factorization[9–11] (NMF) or independent component analysis[12,13] (ICA) upon a set of previously registered spectral measurements (called training spectra) provides a set of vectors, i.e., a linear basis, which can be linearly combined to obtain the spectral estimation. Three of the

four methods we have studied here, the Maloney–Wandell method[6] (which has been widely used by other authors[4,14]), the Imai–Berns method,[15] and the Shi–Healey method,[16] rely on the use of a linear basis. Another way of including *a priori* spectral knowledge is to develop a Wiener pseudoinverse[17,18] (also called direct pseudoinverse[19,20]), where the sensor responses to the known training spectra are then used to construct a matrix that provides unknown spectra from their measured responses. These methods are described in detail in Section 2 and have been compared here because they are the most frequently used[2,4,6,14–29] spectral estimation algorithms to recover illuminant or surface spectra from sensor responses owing to the accurate results they provide.

In Section 4 we present the optimum sensors and their accuracy in reconstructions of the four estimation methods used with various amounts of added noise and comparisons of the influence of nonuniform versus uniform A/D quantization for spectral skylight data representation. We also show the lowest number of training spectra that could be used in each method. We make a comparative study of the speed of each of the four spectral estimation methods as a function of the size of the training set of spectra used in the recovery method. Finally, we compare the efficiency of the different linear bases provided by PCA, ICA, and NMF used with the Maloney–Wandell, Imai–Berns, and Shi–Healey methods to recover skylight spectra and show the optimum number of basis vectors that should be used in each case.

2. SPECTRAL ESTIMATION ALGORITHMS

We simulate the spectral response of CCD camera sensors assuming this response to be linear.[2,14,21–23] If we make this assumption for our multispectral imaging system, we can model its sensor responses using

$$\rho = R^t E, \tag{1}$$

where we have sampled the visible spectrum at N different wavelengths and assumed vector notation for the resulting magnitudes. In Eq. (1) ρ is the column vector representing k sensor responses ($k = 3, 4, 5$, given here the typical dimensionality of natural illuminant spectra[4,7,8]), E is the illuminant spectrum (skylight in our case, ranging from 380 to 780 nm in 5 nm steps, within which we have 81 samples per spectrum) represented by an $N \times 1$ column vector, and R is an $N \times k$ matrix containing the spectral sensitivities of the k sensors at N sampled wavelengths (superscript t denotes its transpose). Any real imaging system is of course affected by noise,[2,4,17,30–32] a fact not explicitly accounted for in Eq. (1). Nevertheless, noise can be represented there as an additive term[2,21,22] that changes the ideal noise-free sensor responses, ρ_{free}, to

$$\rho = \rho_{free} + \sigma, \tag{2}$$

where σ is a k-row vector of uncorrelated components that affect each sensor separately.[4,17,21–23] A good review of sensor noise sources can be found in Yotter and Wilson.[32]

The goal here is to recover the skylight spectra, E, from the calculated sensor responses, ρ. Different estimation methods have tried to solve this problem. As mentioned in

the introduction, it is common to make use of *a priori* knowledge of the spectra we want to recover, with PCA, ICA, or NMF being widely used strategies.[2,4,6–16,24–29] They coincide in providing a set of vectors that can be used to express a given spectrum as a linear combination

$$E = V\epsilon, \tag{3}$$

where V is an $N \times n$ matrix containing the first n vectors used for reconstructing N wavelengths (n is always less than or equal to N and is usually chosen to equal k, the number of sensors, which often gives the best results[15,24,25]). Vector ϵ is an n-rowed vector that contains the coefficients of the linear combination. The first three methods discussed make use of this linear approximation for the spectra.

A. Maloney–Wandell Method
This method[6] simply substitutes Eq. (3) into Eq. (1) to obtain

$$\rho = R^t V\epsilon = \Lambda \epsilon, \tag{4}$$

where Λ is a $k \times n$ matrix that directly transforms the coefficients, ϵ, into the sensor responses, ρ. By calculating Λ's pseudoinverse (denoted by superscript $^+$), we obtain the coefficients for the linear estimate of the spectrum from the camera's sensor responses and can then recover the skylight spectrum

$$E_R = V\Lambda^+ \rho. \tag{5}$$

According to this method the *a priori* information provided by the training spectra is included in matrix V (which contains the basis vectors), which also appears in Λ, as can be seen in Eq. (4). With this method it is also necessary to measure the spectral sensitivities, R, of the k sensors to obtain matrix Λ.

B. Imai–Berns Method
Imai and Berns developed a method[15] for recovering spectral data based directly on a relationship between sensor responses ρ and coefficients ϵ, which now includes a column in ρ_{ts} and ϵ_{ts} for each of the m training spectra (subscript ts stands for training spectra; we will use different values for m in this study, as will be explained later):

$$\epsilon_{ts} = G\rho_{ts}. \tag{6}$$

In this new equation, the system matrix, G, is an $n \times k$ matrix, which is formally similar to Λ^+ in Eq. (5) but is now determined empirically by a least-squares analysis of the training-spectra measurements. Hence it is not necessary to measure the spectral sensitivities, R, of the camera to use this method with real sensor-response measurements.[19] We can estimate matrix G via a least-squares analysis by pseudoinverting the $k \times m$ matrix ρ_{ts}

$$G = \epsilon_{ts}\rho_{ts}^+. \tag{7}$$

In our case the recovered skylight spectrum is simply calculated in this method from the sensor responses, ρ, by

$$E_R = VG\rho. \tag{8}$$

Here, the information provided by the training spectra is included in V and in G.

C. Shi–Healey Method

Shi and Healey[16] designed a very insightful method that allows the use of higher-dimensional models for the reflectance and illuminant spectra in Eq. (3). Although the Maloney–Wandell and Imai–Berns methods can be used with more eigenvectors than sensors ($n > k$), this does not lead to the best results—as we will see later—because a model with $n > k$ does not determine a unique mapping between ρ and ϵ, since E vectors, having different ϵ values, can generate the same ρ vector[16] as a result of loss of information when registering a $n > k$ linear model with just k parameters (the sensor responses). We call S_E the set of vectors, E, generated when varying the n coefficients, ϵ (more than the number of sensors k), and having the same responses, ρ. To associate a sole E_R recovered illuminant vector with a ρ measurement vector, we can select a single vector, E^*, from the set S_E with the constraint of requiring that E^* be the vector in S_E that minimizes the mean-square error calculated throughout the training spectra. In other words, we will choose E^* from a given ρ as that vector that is most similar to a training spectrum among those vectors of S_E that are consistent with both the linear model and the sensor vector, ρ.

Since we have k sensors, given a dimensionality of n for the linear model, we separate the contributions of the last k principal components (denoted by subscript 2) and the remaining $n - k$ first principal components (subscript 1) in Eq. (4):

$$\rho = R^t (V_1 \epsilon_1 + V_2 \epsilon_2), \qquad (9)$$

where V_1 contains the eigenvectors $1, \ldots, n - k$ and V_2 contains the eigenvectors $n - k + 1, \ldots, n$. The vectors ϵ_1 and ϵ_2 contain the corresponding coefficients for the linear estimation. From Eq. (9) we can solve for ϵ_2 in terms of ϵ_1 according to

$$\epsilon_2 = (R^t V_2)^{-1}(\rho - R^t V_1 \epsilon_1), \qquad (10)$$

and substituting into Eq. (3), we get

$$E = V_1 \epsilon_1 + V_2 (R^t V_2)^{-1}(\rho - R^t V_1 \epsilon_1). \qquad (11)$$

From this equation, we can construct an $N \times m$ matrix, E^*, of column vectors of S_E that minimizes the mean-square error throughout the training spectra, which is the solution of a least-squares problem that can be solved for ϵ_1 using pseudoinversion

$$E^* = V_1 \epsilon_1^* + V_2 (R^t V_2)^{-1}(\rho^* - R^t V_1 \epsilon_1^*), \qquad (12)$$

where ρ^* is a $k \times m$ matrix containing the sensor responses, ρ, to the measured spectra, E, repeated in its m columns, and the $(n-k) \times m$ matrix, ϵ_1^*, is given by the equation

$$\epsilon_1^* = (V_1 - V_2 (R^t V_2)^{-1} R^t V_1)^+ (E_{ts} - V_2 (R^t V_2)^{-1} \rho^*), \quad (13)$$

where E_{ts} is an $N \times m$ matrix containing one training spectrum per column. We have constructed an $N \times m$ matrix, E^*, of estimated spectra from the sensor responses, ρ, of a measured spectrum, E. Each column of E^* is related to each column of E_{ts}, containing the training spectra. If we calculate the distance between each column of E^* to each column of E_{ts}, we can choose the estimated spectrum, E_R, as that column of E^* for which this distance is minimum

$$E_R = E_i^*, \qquad (14)$$

in which i selects the column of E^* for which the distance $\|E_i^* - E_{ts_i}\|$ is minimum. The most important disadvantage of this method is that for every given vector response, ρ, we have to calculate m estimated spectra for E^* and choose the minimum of m distances. If m is large the algorithm is extremely slow. We also need to measure accurately the spectral sensitivities, R, of the camera. This method will be used here with $n = k + 1, k + 2, \ldots$ basis vectors, since if we use just k basis vectors, the matrix, V_1, would be zero and Eq. (12) would be exactly the same as Eq. (5) for the Maloney–Wandell method for k sensors and k basis vectors (Λ would be a square $k \times k$ matrix).

D. Wiener Estimation Method

The Wiener estimation method[17–24,26] is formally similar to the Imai–Berns method, but it directly relates sensor responses, ρ, with spectral estimations, E_R, using a matrix (here W). Thus

$$E_R = W \rho. \qquad (15)$$

We can estimate W using a least-squares approach by calculating ρ's pseudoinverse for the training spectra as follows:

$$W = E_{ts} \rho_{ts}^+. \qquad (16)$$

In this method it is not necessary to measure the spectral sensitivities of the camera or to calculate a linear basis of training spectra. The information of the training spectra is included in W, as can be seen in Eq. (16). We must try to build a "robust-to-noise" matrix W (as explained in Section 4) and introduce sensor responses into Eq. (15) to obtain the spectral estimations.

3. SEARCH ALGORITHM

In a previous study[29] it was found that three PCA basis vectors are enough to recover skylight spectra with acceptable accuracy. Assuming this dimensionality for skylight spectral representation based on linear basis vectors, here we have tried to find the optimum set of three to five Gaussian sensors to recover skylight spectra from their responses by varying as much as possible all the parameters defining a Gaussian sensor (central position, width, and relative height) within the typical commercial values available. To this end we focused on the visible range of the spectrum (from 380 to 780 nm) and in each simulation varied the sensors' central positions within this range in 5 nm steps; we also varied their FWHM (full width at half-maximum) from 10 to 250 nm in 5 nm steps and their peak values from 0.5 to 1 in 0.1 steps. We simulated thermal and shot sensor noise as random, normally distributed noise with standard deviations of 1%, 3%, and 5% of the maximum sensor response. These noise levels correspond to signal-to-noise ratios (SNRs) of 40, 30, and 26 dB, respectively, and have proved to be close to the typical values measured in multispectral imaging systems.[2,17,20–23,27] Quantization noise is represented as

that due to A/D uniform conversion at a resolution of 8, 10, and 12 bits. We also compare this uniform quantization noise with some previously compressed quantization noise[28] in Section 4. We developed all these simulations for each of the four methods presented, for three different sizes of the training spectra (as explained in the following section), and for various numbers of basis vectors used with those methods that need them. To appreciate the computational burden involved, let us consider that if we were to undertake an exhaustive search, about 10^{15} different sets would have to be evaluated to find the optimum set for a three-sensor system, a search that would require several days on existing personal computers. This huge number grows if we try to find the best four or five sensors, for which the task is now impractical because the number of possible sets increases by factors of 10^4 and 10^8, respectively. Faced with such daunting computational challenges, we turned to *simulated annealing* algorithms,[3,4,14,17,33] which have been widely used as search algorithms in physics and speed up considerably the search for optimum solutions to a system with many different sets of sensors. This search algorithm requires the minimization of one single-cost function (the energy of the system[4]), so we must be careful in choosing the metric or cost function to be minimized according to a suitable optimization criterion. The key question is what metric to use. For our problem essentially two kinds of metrics exist: colorimetric and spectral.[5,34] Colorimetric metrics, such as those proposed by the CIE (CIELUV, CIELAB, CIE94, and CIEDE2000), approximate color differences observed by the human eye. Spectral metrics are those that measure the distance between two spectral curves, such as the root-mean-square error (RMSE) or GFC ("goodness-of-fit coefficient"),[29] which uses Schwartz's inequality, a widely accepted[5,34,35] index of similarity between two spectra. These metrics distinguish between metamers but do not take human vision into account. However, some new spectral metrics have been proposed for comparing spectra that do take properties of the human visual system into account, such as weighted RMSE (WRMSE) with the diagonal of Cohen's matrix[34] R, or Viggiano's spectral comparison index[35] (SCI). Finally, another metric widely used in solar radiation measurements is the percentage of the integrated irradiance error[36] [IIE(%)] across the visible spectrum.

We have shown in a previous publication[4] how the spectral sensitivity of the optimum sensors depends much on the metric used if we minimize only one of the metrics described above in our optimization. Imai *et al.*[34] suggest that "mononumerosis" should be avoided when evaluating the quality of spectral matches. By this they mean that *several* metrics should be used to assess color reconstruction from both colorimetric and spectral standpoints. We have to use a single cost function when developing a simulated annealing algorithm, an approach that may seem to contradict the recommendations of Imai *et al.*[34] but in fact does not, because we actually use a simple single-cost function or metric that combines several metrics at once. We use GFC as a spectral metric, CIELAB ΔE^*_{ab} as a colorimetric cost function, and IIE(%) as a metric for comparing the integrated power in the visible spectrum of natural illuminants. In principle, this metric should approach zero for near-perfect matches and give approximately the same weight to the GFC, CIELAB ΔE^*_{ab}, and IIE(%) metrics. Our colorimetric and spectral combined metric (CSCM) has proved to be satisfactory for comparing skylight spectra and is calculated[4,5] by

$$CSCM = Ln(1 + 1000(1 - GFC)) + \Delta E^*_{ab} + IIE(\%),$$

(17)

where Ln means natural logarithm. The chief advantage of this metric is that it quantifies spectral mismatches among metamers, perceptual differences in color matches, and differences in such integrated radiometric quantities as radiance and irradiance. Though this metric may not avoid "mononumerosis," it clearly combines the properties of various metrics relevant to skylight spectra and thus is a good candidate for developing an annealing search algorithm. Hence, optimum sensors will be those that minimize the mean value of the CSCM metric for differences between original and recovered spectra over the complete skylight spectra test set, as we show in the next section.

4. RESULTS

First we present in Subsection 4.A the spectral shape (position, width, and height) of the optimum sensors found for each reconstruction algorithm in two of the noise situations described above (for SNRs equal to 40 and 26 dB, uniform quantization with 12 bits is used here) and use different numbers of basis vectors in those methods that require them (here we use those basis vectors provided by PCA). We compare these optimum spectral sensitivities when using three sizes of the training set of spectra, m, to perform PCA and build system matrices: 1567, 156, and 20. The complete 1567 skylight radiance training spectra were taken in Granada,[29] Spain ($37°10'$N, $3°36'$W, elevation 680 m) over two years at many different solar elevations, with different azimuths, and during different seasons of the year; each spectrum ranged from 380 to 780 nm in 5 nm steps. We used the complete set and two subsets of 156 and 20 spectral curves randomly extracted from it just once to train the system. The original set and the two subsets of skylight spectra proved to have a high variety in the spectral shapes and colorimetric characteristics in all cases.[29,37] We used the complete set of 1567 skylight spectra as a test set in all the recovery experiments.

In Subsection 4.B we compare the accuracy of the reconstructed skylight SPDs of the complete test set of 1567 spectra when they are recovered using PCA basis vectors (if needed) and the optimum sensors found for each method, bearing in mind the GFC, ΔE^*_{ab}, and CSCM metrics described in Section 3. We show that all the methods studied provide high-quality skylight recovered spectra, measured with various metrics, from the responses of a few sensors affected by noise. We also present in Subsection 4.C some results concerning the optimum number of PCA basis vectors to be used with each method in each noise situation and compare the accuracy achieved when using other linear bases provided by ICA and NMF.

In Subsection 4.D we make a brief study of the speed of each recovery method as a function of the training-set size, and finally we compare the performance of skylight SPD recovery using uniform and nonuniform quantization in the A/D conversion.[38]

A. Spectral Profile of Optimum Sensors

If we study the peak location and FWHM of the optimum sensors for the Maloney–Wandell method using PCA basis vectors, we see that they are almost the same for every number of basis vectors used, for every training-set size, and for every noise level. This behavior is desirable for developing a practical multispectral system. As other authors have noted,[4,14,21–23] sensor sensitivity curves tend to sharpen slightly when the noise is high (i.e., low SNR). Not surprisingly,[4] the curves also sharpen as the number of sensors increases (i.e., as we approach a narrowband hyperspectral imaging system). We show these properties in Fig. 1 for $k = 3, 4, 5$; $m = 1567$; and 12-bit quantization.

For the Imai–Berns method with PCA basis vectors (Fig. 2), the optimum sensors perform very differently according to whether the number of sensors, k, is three or four or five, although there is no significant change in their shapes if we change m within each value of k. With four sensors the decrease in SNR (caused by an increase in noise levels) does not involve any meaningful change in the spectral shape of the optimum sensors (they only seem to sharpen slightly, as in the Maloney–Wandell method). Nevertheless, with three sensors an increase in noise results in a significant widening of the sensors and a shift of some sensors to the blue end of the visible spectrum, as shown in Fig. 2 for $m = 1567$. A similar increase in noise with five sensors produces hardly any change in FMWH owing to its already small value, but some sensors also shift toward the blue. Some authors[20–23] have proved that the combination of optimum sensors must be found for each noise level owing to a lack of robustness to noise of those optimum filters found for low-noise situations (i.e., the optimum sensors found in low-noise situations give very poor recoveries when noise rises). In other words, the shape of the optimum sensors may change significantly if noise rises. Some authors have tried to measure this robustness to noise in various ways. Hardeberg[2] calculated the condition number (the ratio between the highest and the lowest singular value) of the transformation matrix. Shimano[21–23] calculated the singular values of a matrix known as $SLV\Lambda^{1/2}$, where S represents the spectral sensitivities, L is a diagonal matrix for the illuminant, V is a matrix composed of PCA eigenvectors, and Λ is a diagonal matrix with the correspondent eigenvalues. Day[20] argued, for the Imai–Berns method, that the robustness to noise of the transformation matrix VG can be estimated empirically from the plot of each coefficient of this matrix as a function of wavelength. It should be noted that in the Imai–Berns method, VG is an $N \times k$ matrix that directly transforms sensor responses to SPD and therefore that summing up the result of multiplying each wavelength-dependent coefficient by its corresponding sensor response provides the recovered spectra. In Fig. 3 we show that this transformation for the low-noise three optimum sensors (solid curve) is composed of steep slopes (note that the absolute value of its derivative would be
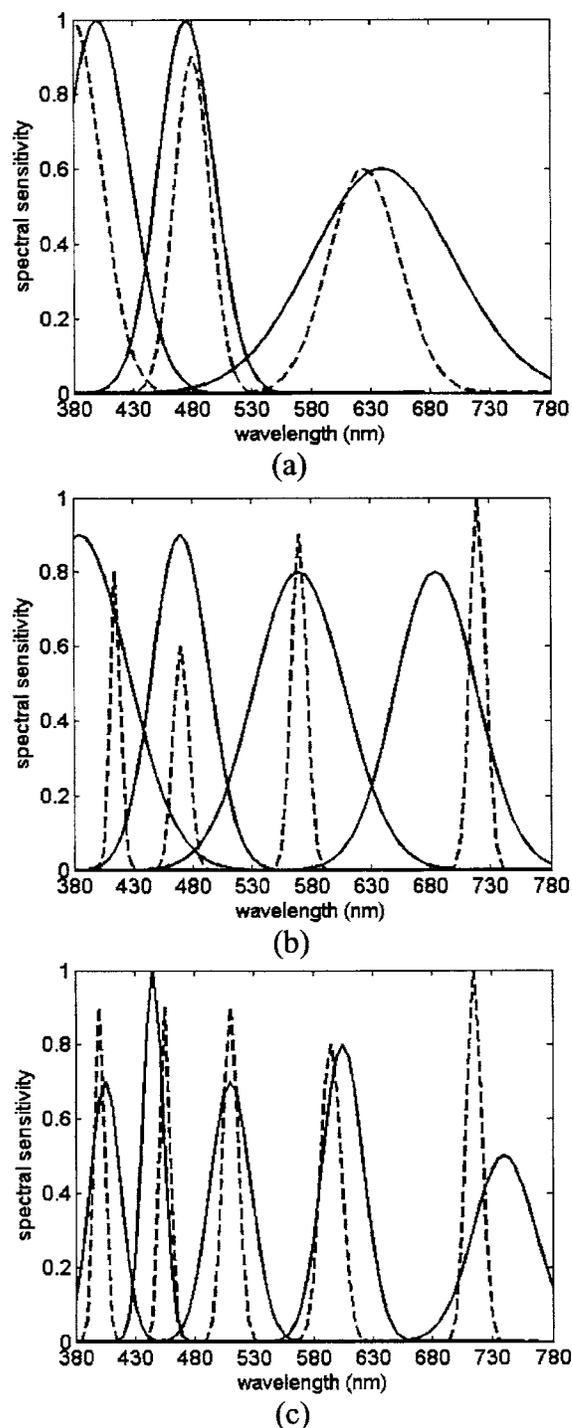

Fig. 1. (a) Optimum three sensors, (b) four sensors, and (c) five sensors for Maloney–Wandell[6] method with $m = 1567$ training spectra. Equal numbers of sensors and PCA basis vectors are used. Solid curves denote SNR=40 dB, and dashed curves denote SNR=26 dB.

high), which in turn would amplify small differences caused by noise. The transformation obtained for high-noise three optimum sensors (dotted curve) is smoother, resulting in a matrix that is more robust to noise.

In Fig. 4 we show the optimum sensors found for the Shi–Healey method with PCA basis vectors and $m = 1567$, although the only significant dependence in their spectral

sensitivity found by decreasing m was a small sharpening. The optimum sensors with this method are very peculiar since they seem to fall equidistantly within the visible range and are very narrowband, which indicates that they could easily be obtained using a liquid-crystal tunable filter (LCTF) with narrowband modes.[2] The optimum sensors with this method also sharpen concomitantly
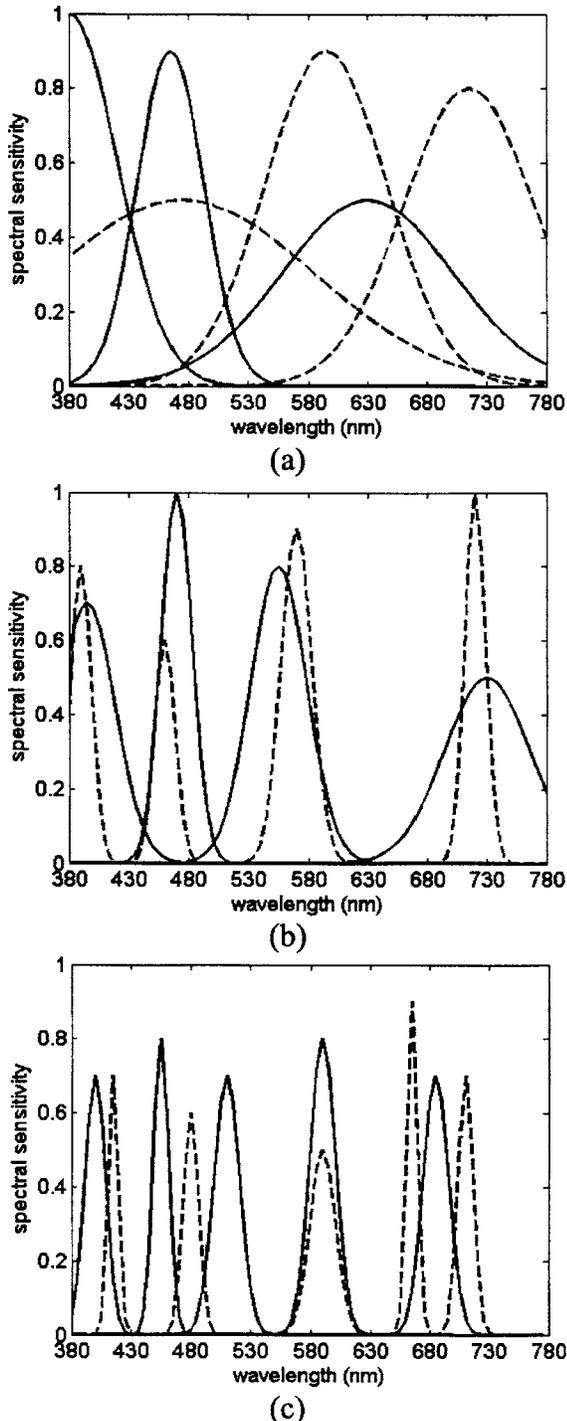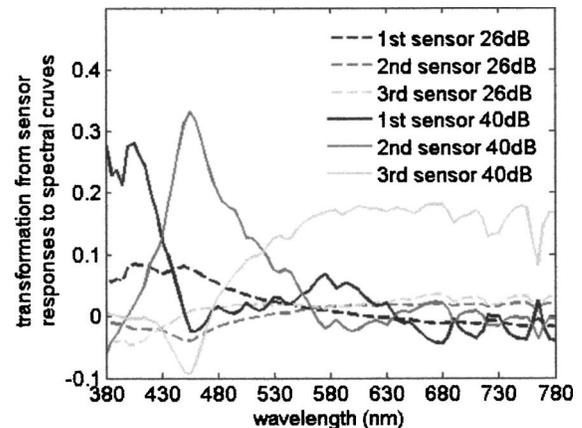

Fig. 3. Plot of the transformation matrix versus wavelength at various noise levels. Matrix coefficients are given by the optimum sensors of the Imai–Berns[15] method for three sensors, three PCA basis vectors, and $m = 1567$.

with a rise in noise, as they do in the Maloney–Wandell method. When five sensors are involved, some of them shift to the blue end of the spectrum with high noise, as they do in the Imai–Berns method.

Finally, the optimum sensors for the Wiener estimation method look very similar to those obtained with the Maloney–Wandell method in every situation, although this method requires the use of a linear basis of reduced dimensions and a knowledge of the spectral sensitivities of the camera, whereas the Wiener method does not. The sharpening of the optimum sensors concomitantly with noise is also notable, as shown in Fig. 5 for $m = 1567$ (once more, no important changes occurred in the optimum spectral sensitivities when m decreased).

We can appreciate visually in Fig. 1, 2, 4, and 5 how the peak positions of the optimum sensors found for the four methods seem to be similar to the positions of the usual absorption bands typically found in skylight spectral curves (see Fig. 6). We may conclude that the spectral recovery algorithms studied here try to locate their optimum sensors in those positions of minimum smoothness in the spectral curves in an attempt to sample accurately the discontinuities in the absorption bands.

B. Accuracy of Spectral Reconstructions

The values for the GFC, CIELAB ΔE_{ab}^*, and CSCM metrics obtained in the spectral reconstructions of the complete test set of 1567 skylight spectra with each of the four methods described above using the optimum sensors found for them are set out in Table 1. We use uniform 12-bit quantization in this section. For the Maloney–Wandell and Imai–Berns methods, we show the results when we used equal numbers of PCA basis vectors and sensors. We did this because it led to better values for all the metrics used—as we show later—thus giving better spectral and colorimetric reconstructions of the skylight SPDs, as other authors have found before.[4,6,14–16,25] Since the Shi–Healey method is designed to work with a larger dimensionality, more PCA basis vectors are used (here we show the results when $n = k + 2$ for this method). The results of this study for the Maloney–Wandell, Imai–Berns, Shi–Healey, and Wiener (in this case, no basis vectors are

Fig. 2. (a) Optimum three sensors, (b) four sensors, and (c) five sensors for Imai–Berns[15] method with $m = 1567$ training spectra. Equal numbers of sensors and PCA basis vectors are used. Solid curves denote for SNR=40 dB, and dashed curves denote SNR =26 dB.

needed) methods are set out in Table 1. We show in each row the results obtained using a different number of sensors for GFC, CIELAB ΔE_{ab}^*, and CSCM metrics. We separate into columns three cases of simulated noise and the number m of training spectra used in every noise situation.

We can see for the Maloney–Wandell method how an increase in the number of sensors from three to five re-
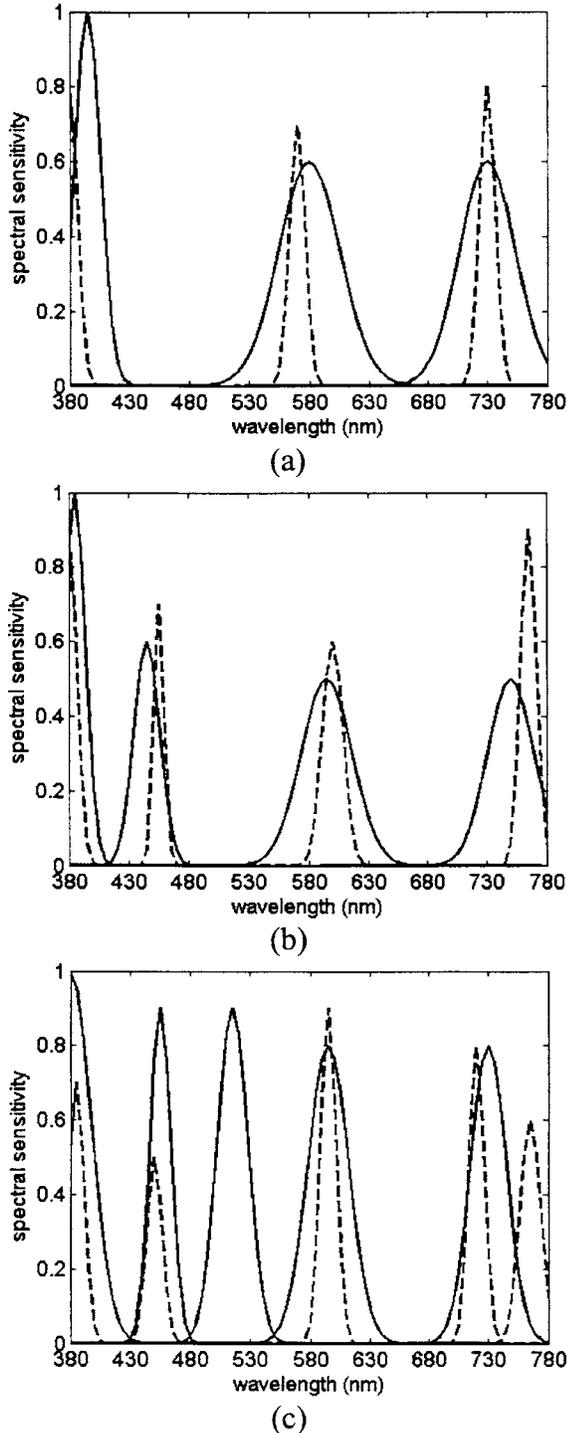

Fig. 4.   (a) Optimum three sensors, (b) four sensors, and (c) five sensors for Shi–Healey[16] method with $m = 1567$ training spectra. Here $n = k + 2$ PCA vectors are used. Solid curves denote SNR $= 40$ dB, and dashed curves denote SNR $= 26$ dB.
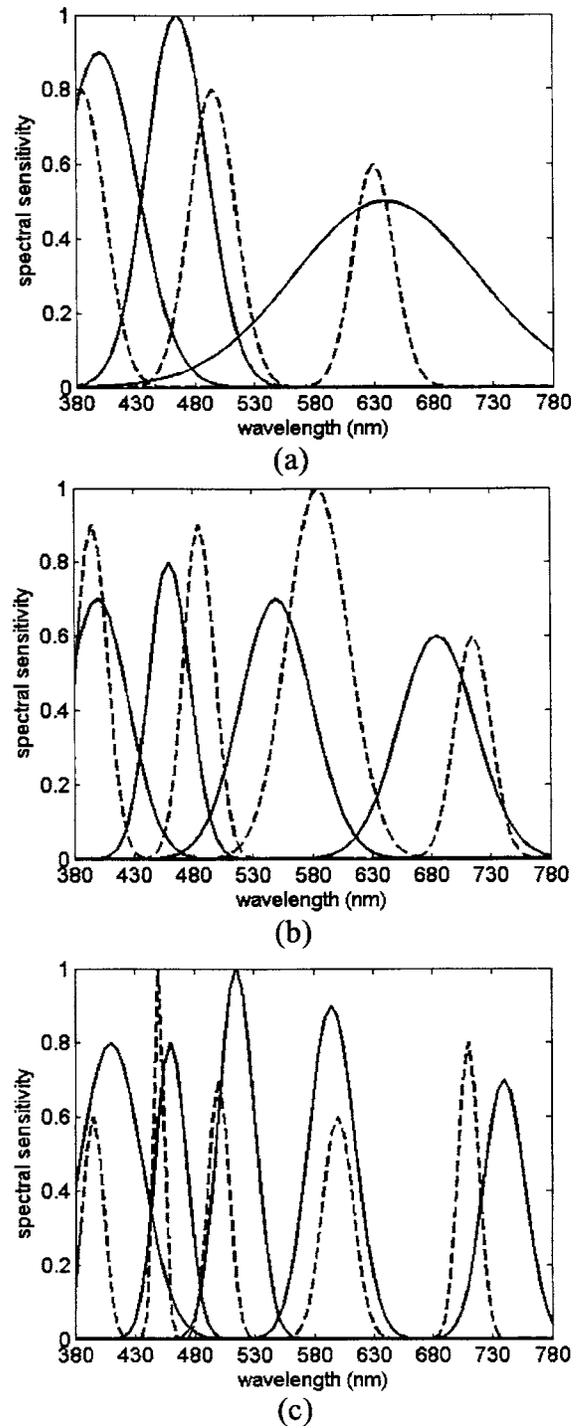

Fig. 5.   (a) Optimum three sensors, (b) four sensors, and (c) five sensors for the Wiener method[18] with $m = 1567$ training spectra. Solid curves denote SNR $= 40$ dB, and dashed curves denote SNR $= 26$ dB.

sults in better values for the metrics used in every noise situation. Nevertheless, with low SNRs the improvement obtained when increasing the number of sensors, k, is less if we go from four to five sensors than it is when going from three to four sensors. This same tendency toward increasing k also applies to the Imai–Berns method, the results of which are also set out in Table 1. This latter method gives better results than the Maloney–Wandell

Table 1. Mean Values±Standard Deviations for Various Metrics and Noise Situations When Recovering the Complete Test Set of 1567 Skylight Spectra Using the Optimum Sensors Found in Each Case with Various Sizes *m* of the Training Set of Spectra

Method	Sensors	Metric	40 dB			30 dB			26 dB		
			m = 1567	*m* = 156	*m* = 20	*m* = 1567	*m* = 156	*m* = 20	*m* = 1567	*m* = 156	*m* = 20
Maloney-Wandell	3 [a]	GFC	0.9994±0.0012	0.9994±0.0012	0.9993±0.0018	0.9988±0.0014	0.9986±0.0015	0.9986±0.0020	0.9978±0.0022	0.9976±0.0026	0.9979±0.0027
		ΔE^{*}_{ab}	0.8100±0.5652	0.8253±0.5475	0.8471±0.5780	1.1128±0.6554	1.1930±0.7290	1.1729±0.6518	1.5283±0.9397	1.5020±0.8601	1.4408±0.7580
		CSCM	2.0125±1.0836	2.0887±1.1111	2.0375±1.1637	4.0604±2.1096	4.1479±2.1333	4.0540±2.1303	6.1107±3.2926	6.2546±3.3288	6.1138±3.3531
	4 [a]	GFC	0.9997±0.0003	0.9997±0.0003	0.9997±0.0003	**0.9992±0.0006**	0.9991±0.0006	0.9991±0.0006	0.9980±0.0016	0.9982±0.0014	0.9980±0.0015
		ΔE^{*}_{ab}	0.6033±0.3512	0.5991±0.3445	0.5829±0.3335	0.9522±0.5032	0.9567±0.5286	0.9877±0.5482	1.3533±0.7084	1.3320±0.6958	1.3348±0.7011
		CSCM	1.4725±0.6926	1.4846±0.7046	1.4831±0.7208	3.4594±1.7657	3.4385±1.6999	3.4594±1.7007	5.4057±2.8011	5.4808±2.8623	5.4401±2.7033
	5 [a]	GFC	**0.9998±0.0001**	**0.9998±0.0001**	**0.9998±0.0001**	**0.9992±0.0006**	0.9991±0.0006	**0.9992±0.0006**	0.9980±0.0015	0.9980±0.0014	**0.9981±0.0015**
		ΔE^{*}_{ab}	0.3496±0.1830	0.3397±0.1764	**0.3370±0.1749**	0.9247±0.4694	0.9183±0.4821	**0.9032±0.4594**	**1.3957±0.6956**	1.4943±0.7619	1.4447±0.7647
		CSCM	**1.0701±0.4956**	1.1235±0.5539	1.0804±0.5352	**3.1745±1.4771**	3.2934±1.6028	3.2405±1.5367	5.2575±2.4056	5.2783±2.4434	**5.2395±2.4878**
Imai-Berns	3 [a]	GFC	0.9993±0.0012	0.9993±0.0012	0.9993±0.0018	0.9981±0.0022	0.9982±0.0021	0.9980±0.0026	0.9972±0.0030	0.9970±0.0030	0.9972±0.0031
		ΔE^{*}_{ab}	0.7725±0.5104	0.8484±0.5946	0.8415±0.5890	1.1219±0.6580	1.1195±0.6270	1.1848±0.6931	1.4748±0.9059	1.5389±0.9456	1.4868±0.8635
		CSCM	2.0089±1.0866	2.0685±1.1334	2.0534±1.2000	3.6348±1.8038	3.6257±1.7812	3.6670±1.8030	5.1959±2.8922	5.3481±2.8313	5.4909±2.7111
	4 [a]	GFC	0.9997±0.0003	0.9997±0.0003	0.9997±0.0003	0.9992±0.0006	0.9991±0.0007	0.9990±0.0007	0.9982±0.0020	0.9982±0.0014	0.9982±0.0020
		ΔE^{*}_{ab}	0.5721±0.3276	0.5669±0.3225	0.5846±0.3209	0.9591±0.5161	0.9723±0.5077	1.0356±0.5906	1.2780±0.6927	1.4028±0.7768	1.4630±0.7856
		CSCM	1.4730±0.7046	1.4791±0.7269	1.4987±0.7289	3.4413±1.7031	3.4844±1.7002	3.5106±1.6668	5.2884±2.8253	5.4192±2.8545	5.2509±2.5917
	5 [a]	GFC	**0.9998±0.0001**	**0.9998±0.0001**	**0.9998±0.0001**	**0.9992±0.0005**	**0.9992±0.0005**	**0.9992±0.0006**	0.9979±0.0017	0.9982±0.0014	**0.9985±0.0012**
		ΔE^{*}_{ab}	**0.3571±0.1792**	0.3645±0.1892	0.3816±0.2032	0.9291±0.4478	0.9319±0.4815	**0.9084±0.4539**	**1.4078±0.7814**	1.4489±0.7758	1.4400±0.7935
		CSCM	**1.1034±0.5340**	1.1365±0.5725	1.1356±0.5581	**3.1452±1.4183**	3.3012±1.6668	3.2431±1.5515	5.1244±2.4092	5.1662±2.4734	**5.1072±2.5020**
Shi-Healey	3 [b]	GFC	0.9997±0.0003	0.9996±0.0005	0.9987±0.0017	0.9991±0.0010	0.9990±0.0016	0.9988±0.0023	0.9981±0.0020	0.9981±0.0021	0.9981±0.0028
		ΔE^{*}_{ab}	0.5730±0.4611	0.6967±0.5384	0.6316±0.4208	**0.8832±0.4889**	0.8890±0.4967	1.1735±0.8138	1.3389±0.7019	1.3161±0.7102	1.4832±0.9410
		CSCM	1.1727±0.7586	1.4901±1.0324	2.0429±1.0811	2.5490±1.4844	2.6150±1.5585	3.0210±1.6681	3.8812±2.1784	3.8049±2.0534	3.9562±2.0785
	4 [b]	GFC	0.9998±0.0001	0.9998±0.0004	0.9997±0.0013	0.9992±0.0006	0.9992±0.0007	0.9990±0.0023	**0.9984±0.0011**	0.9983±0.0013	0.9981±0.0027
		ΔE^{*}_{ab}	0.3669±0.2180	0.4456±0.3094	0.5420±0.4360	0.8840±0.4819	0.8894±0.4970	0.8991±0.5929	**1.3024±0.6822**	1.3096±0.7299	1.3241±0.7802
		CSCM	0.9346±0.4894	1.0987±0.7234	1.5045±1.3626	2.4704±1.2324	2.5011±1.2186	2.6105±1.3912	**3.6070±1.7733**	3.6710±1.8168	3.8736±2.0198
	5 [b]	GFC	**0.9999±0.0001**	0.9998±0.0005	0.9997±0.0009	**0.9993±0.0005**	0.9992±0.0005	0.9988±0.0025	0.9981±0.0013	0.9982±0.0011	0.9970±0.0024
		ΔE^{*}_{ab}	**0.3615±0.1983**	0.3791±0.2046	0.4646±0.2711	**0.9109±0.5045**	0.9337±0.5440	1.0216±05914	1.3725±0.7638	1.3308±0.7277	1.5407±0.8005
		CSCM	**0.8575±0.4171**	1.0537±0.6105	1.3610±0.7250	**2.2915±1.0790**	2.4337±1.1714	3.0265±1.4449	3.9762±1.8952	3.9648±1.8174	4.7803±2.1479
Wiener	3	GFC	0.9994±0.0012	0.9993±0.0012	0.9992±0.0018	0.9985±0.0013	0.9985±0.0014	0.9985±0.0017	0.9973±0.0021	0.9974±0.0025	0.9977±0.0027
		ΔE^{*}_{ab}	0.7873±0.5240	0.7740±0.5051	0.8757±0.5760	1.1093±0.6222	1.0559±0.5711	1.0172±0.5413	1.6387±0.9101	1.4439±0.7997	1.4872±0.7656
		CSCM	1.9882±1.0422	2.0499±1.1038	2.1259±1.1779	3.9327±1.8896	3.8940±1.8102	3.8921±1.9276	5.9300±2.7607	6.0421±3.1725	5.9929±3.2187
	4	GFC	0.9997±0.0003	0.9997±0.0003	0.9997±0.0003	0.9992±0.0006	0.9992±0.0006	0.9992±0.0006	0.9980±0.0016	**0.9982±0.0013**	**0.9982±0.0014**
		ΔE^{*}_{ab}	0.5683±0.3159	0.5717±0.3251	0.5735±0.3181	0.9542±0.5096	0.9592±0.5014	0.9657±0.5169	1.4628±0.8502	1.3707±0.7364	**1.3288±0.7035**
		CSCM	1.4539±0.6839	1.4604±0.7041	1.4537±0.6898	3.4429±1.7070	3.4186±1.7301	3.3701±1.6212	5.3745±2.6812	5.3681±2.7878	5.3167±2.6276
	5	GFC	**0.9998±0.0001**	**0.9998±0.0001**	**0.9998±0.0001**	**0.9993±0.0006**	**0.9993±0.0005**	**0.9993±0.0006**	0.9980±0.0014	0.9981±0.0014	**0.9982±0.0012**
		ΔE^{*}_{ab}	**0.3446±0.1795**	0.3661±0.1967	0.3626±0.1935	**0.8302±0.4275**	0.8813±0.4377	0.8884±0.4614	1.4010±0.7082	1.4392±0.7196	1.3577±0.6695
		CSCM	1.0983±0.5165	**1.0928±0.5311**	1.1181±0.5445	3.1439±1.6343	3.1311±1.5465	**3.0790±1.5236**	**5.0855±2.5114**	5.3258±2.5206	5.1500±2.4326

Note: Uniform 12-bit quantization was used. The best results for each metric within each method and each noise situation are in bold type.
[a] Equal numbers of sensors and PCA basis vectors are used.
[b] A number of PCA vectors $n=k+2$ are used.

method when the noise rises, the improvement being more noticeable with three sensors. The Imai–Berns method has the additional advantage of rendering it unnecessary to measure the spectral sensitivities of the sensors, which usually leads to systematic errors in the Maloney–Wandell method if this task is not undertaken with great precision. With both of these methods, the value of m plays little part in the accuracy of the reconstructions (just as we found in the shape of the optimum sensors). In a previous work,[4] we showed for the Maloney–Wandell method that the optimum sensors found with the 1567 skylight spectra as a training set provide accurate spectral recovery results when tested with a different set of 240 spectra measured in a different place. Here, we obtain the same results for every value of m (except in the case of the Shi–Healey method, as we show later), proving the reliability of the results even for spectra not included in the training set and, hence, for spectra that could be measured at a different location.

The results concerning the Shi–Healey method are shown in Table 1 for a number of PCA basis vectors $n = k + 2$. This method provides the best spectral reconstructions of skylight compared with the other three methods tested, although it is extremely slow, as we shall see later. Owing to the individual comparison of the spectra involved in this method (as explained in Section 2), it is always better to use as many training spectra as possible, while the other methods seem to behave similarly for any value of m. It can also be seen that an increase in the number of sensors does not lead to better spectral recoveries when the noise present in the system is high (for low SNRs), a result already found in the other methods and by other authors.[4,21,27] This can be appreciated by noting that the improvement achieved in noise-free simulations when increasing the number of sensors, k, is negligible if
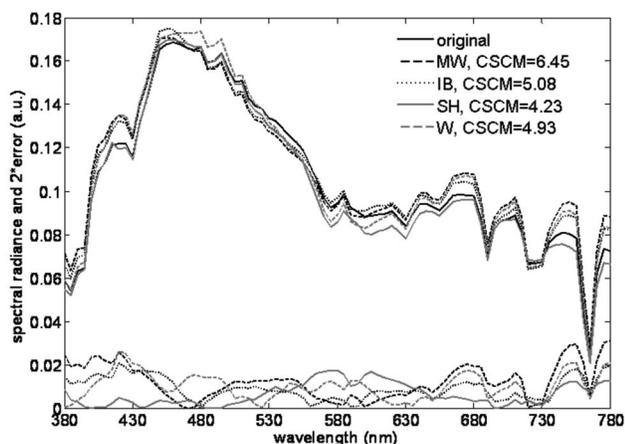

Fig. 6. Skylight spectral radiance and the double of the corresponding spectral error curves for the 95th percentile of the CSCM metric and the Maloney–Wandell[6] method, which is recovered with the four methods studied (MW, Maloney–Wandell[6]; IB, Imai–Berns[15]; SH, Shi–Healey[16]; W, Wiener[17]). Five sensors are used with a SNR of 30 dB, 12-bit quantization, and $m = 156$. Five PCA basis vectors are used with the Maloney–Wandell[6] and Imai–Berns[15] methods, while six PCA vectors are used with the Shi–Healey[16] method.

k is already from four to seven, for example[21,27] (the particular numbers of sensors depend on system hardware

and on the shapes of the spectral data imaged), while the individual noise contributed by each sensor makes the total noise effect considerable in this situation.

The Wiener method produces slightly better results than either the Maloney–Wandell or Imai–Berns method in almost every situation (Table 1), with the additional advantage of not having to calculate either a linear basis or camera sensitivity, R. The behavior of the Wiener method when noise rises is the same as that found with the Maloney–Wandell method; hence the previous discussion is also valid for this latter method. We also see a small dependence with the training-set size, m, in the accuracy achieved with the Wiener estimation method.

In Fig. 6 we show an example of a skylight spectrum reconstructed using the optimum sensors found with each of the four methods studied here and using five sensors, $m = 156$ training spectra, an SNR of 30 dB, and 12 bits for quantization. The sample of spectral skylight chosen for this figure is the 95th percentile for the CSCM metric and the Maloney–Wandell method with five sensors and five basis vectors. We chose this curve since the Maloney–Wandell method is the one that gives the highest best mean value for the CSCM metric (see Table 1). Five PCA vectors were used with the Maloney–Wandell and Imai–Berns methods, while six PCA vectors were used with the Shi–Healey method since these give the best results, as we describe in Subsection 4.C. It can be seen in Fig. 6 that all the skylight SPDs reconstructed from the responses of five sensors are very faithful to the original curve measured with a spectroradiometer, especially those reconstructed with the Shi–Healey and Wiener methods. In particular, they conserve the absorption spiky bands typical of skylight spectra. Thus we may be confident that all the methods studied provide high-quality recovered skylight spectral curves.

C. Basis Vectors

Here we study the optimum number of PCA basis vectors, n, to be used in each recovery method (except the Wiener estimation method, where no basis vectors are needed) as a function of the number, k, of sensors and the noise present in the system ($k = 3, 4, 5$ here as usual in this paper). We used $n = 3, 4, 5$ for the Maloney–Wandell and Imai–Berns methods and $n = 4, \ldots, 8$ for the Shi–Healey method, since this is sufficient to represent the dependence on n of all these methods. In Fig. 7 we show the mean value throughout the complete 1567 skylight-spectra test set for the CSCM metric as a function of $k - n$, the difference between the number of sensors and basis vectors used. The CSCM values represented in Fig. 7 were obtained after recovering the test spectra using the optimum sensors found in each situation, with $m = 156$ as the training-set size and with the usual three situations of added noise used in this study. It can be seen that with the Maloney–Wandell and Imai–Berns methods, the lowest values for the CSCM metric are almost always obtained if $n = k$, particularly when the noise in the system is low. With the Shi–Healey method an increase in the number of vectors, n, over the number of sensors, k, is favorable up to a certain limit, which is usually $n = 7$ for high SNRs and $n = 6$ when the noise rises, whatever the number of sensors used. It can also be seen in Fig. 7 that
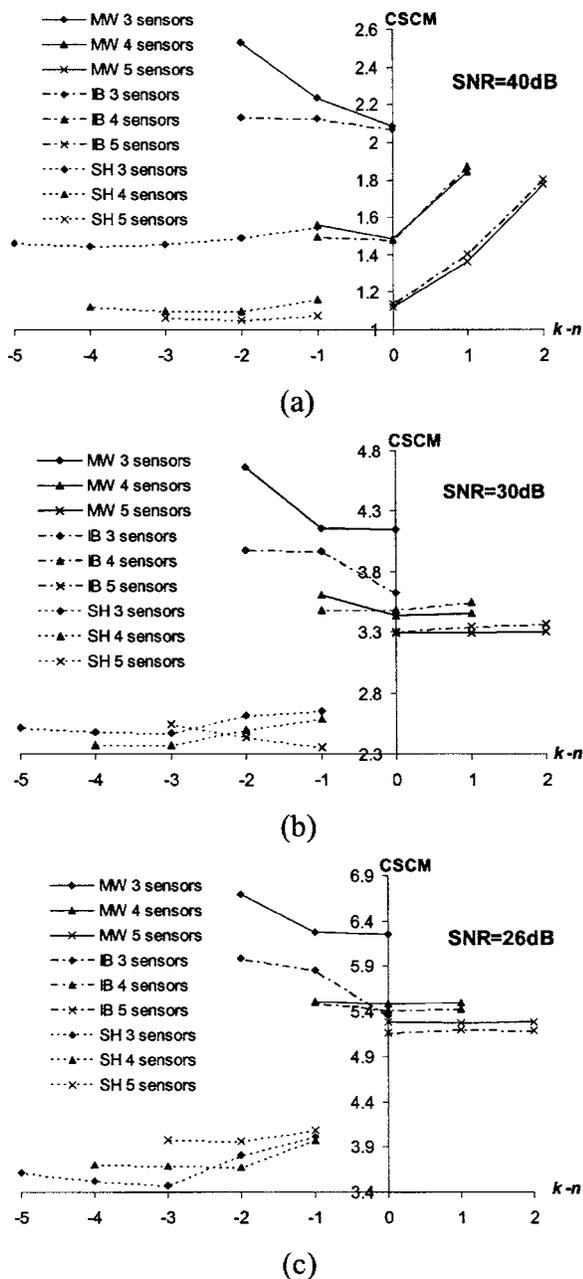
equal to 30 dB, using a training-set size of $m = 156$ spectra and the three estimation methods that require the use of a linear basis. We used $n = 3$ NMF vectors for the Maloney–Wandell and Imai–Berns methods and $n = 5$ NMF vectors for the Shi–Healey method, since the results obtained with NMF vectors are very similar to those obtained for PCA vectors, as we show below. A higher num-
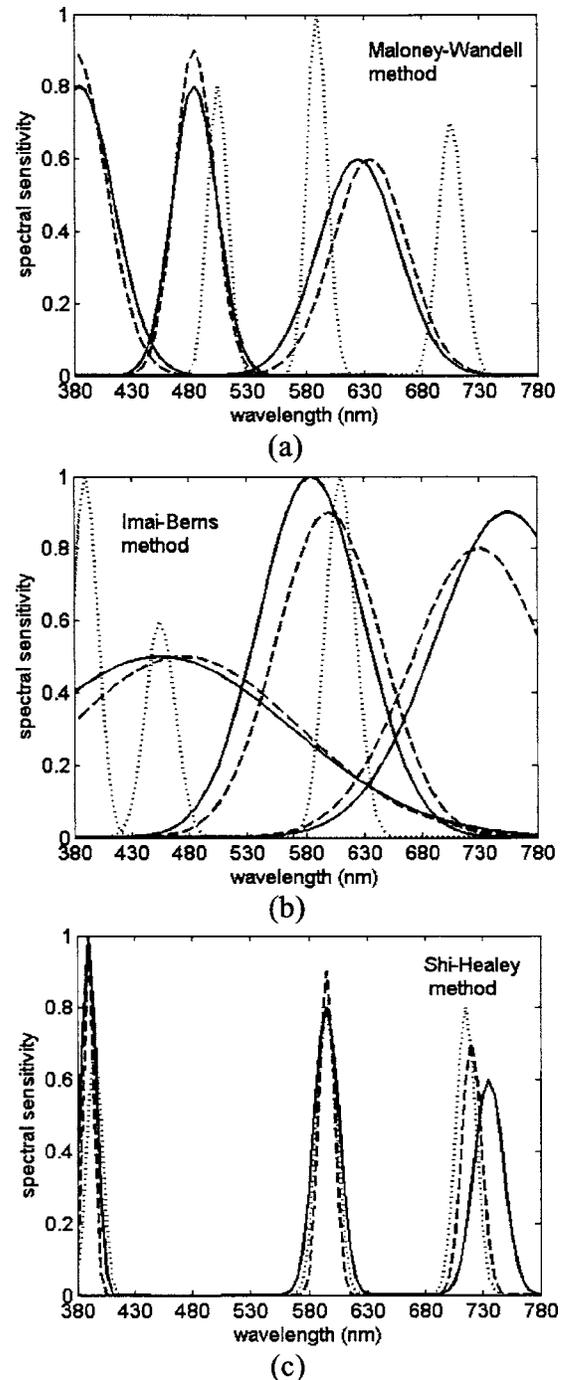

Fig. 7. Mean values for the CSCM metric when recovering the complete test set of skylight spectra with the optimum sensors found using $m = 156$ and different numbers of PCA basis vectors with three methods (MW, Maloney–Wandell;[6] IB, Imai–Berns;[15] SH, Shi–Healey[16]). Uniform 12-bit quantization was used. (a) SNR = 40 dB, (b) SNR = 30 dB, (c) SNR = 26 dB. Note the different vertical axis scale in each case.

with the Shi–Healey method an increase in the number of sensors does nothing to improve the CSCM metric when noise is high (i.e., low SNR), since the values for the CSCM metric with five or four sensors are poorer than those for three sensors, as discussed in Subsection 4.B.

We also compare the optimum sensors and accuracy in the spectral recoveries when we used NMF and ICA basis vectors, compared with those presented for PCA basis vectors for the case of three sensors ($k = 3$). In Fig. 8 we show the optimum three sensors obtained with each of the linear bases provided by PCA, NMF, and ICA with a SNR

Fig. 8. Optimum three sensors for (a) Maloney–Wandell,[6] (b) Imai–Berns,[15] and (c) Shi–Healey[16] methods with $m = 156$ training spectra at SNR = 30 dB and 12-bit uniform quantization. In (a) and (b) the solid curves denote three PCA basis vectors and the dashed curves denote three NMF basis vectors. In (c) the solid curves denote five PCA basis vectors and the dashed curves denote five NMF basis vectors. Dotted curves denote nine ICA basis vectors in all the cases.

**Table 2. Mean Values±Standard Deviations for Various Metrics When
Recovering the Complete Test Set of 1567 Skylight Spectra Using
the Optimum Three Sensors Found in Each Case[a]**

Method	Linear Basis	n	GFC	ΔE^*_{ab}	CSCM
Maloney-Wandell	PCA	3	0.9986±0.0015	1.1930±0.7290	4.1479±2.1333
	NMF	3	0.9986±0.0013	1.2389±0.6804	4.0643±2.1118
	ICA	3	0.9984±0.0015	1.0861±06449	3.1473±1.4617
		6	0.9990±0.0025	1.0174±0.6905	2.6387±1.8315
		9	0.9990±0.0027	1.0125±0.7166	2.6255±1.9525
		12	0.9990±0.0019	0.9935±0.6471	2.6249±1.8808
Imai-Berns	PCA	3	0.9982±0.0021	1.1195±0.6270	3.6257±1.7812
	NMF	3	0.9982±0.0019	1.2389±0.7691	3.7764±1.9498
	ICA	3	0.9949±0.0119	1.6535±1.5041	5.1594±3.4341
		5	0.9965±0.0082	1.3930±1.2161	4.2487±2.7396
		9	0.9971±0.0048	1.0853±0.7866	3.6178±2.1217
		15	0.9982±0.0035	0.9473±0.6240	3.0226±1.8637
		18	0.9983±0.0033	0.8998±0.5769	2.8879±1.8294
		21	0.9986±0.0029	0.9116±0.5551	2.7692±1.7772
		24	0.9987±0.0026	0.9135±0.5443	2.6930±1.6982
Shi-Healey	PCA	5	0.9990±0.0016	0.8890±0.4967	2.6150±1.5585
	NMF	5	0.9990±0.0010	0.9723±0.6065	2.6697±1.4481
	ICA	5	0.9991±0.0010	1.0498±0.6831	2.6955±1.5323
		6	0.9991±0.0012	1.0334±0.6865	2.5142±1.4284
		9	0.9989±0.0021	1.0210±0.7334	2.4980±1.5535
		12	0.9990±0.0013	1.0401±0.6970	2.4978±1.5208
		15	0.9990±0.0014	1.0258±0.6888	2.4389±1.4649
		18	0.9990±0.0012	1.0167±0.6708	2.4206±1.3843
		21	0.9990±0.0014	1.0051±0.6772	2.3725±1.4810

[a]SNR=30 dB and 12-bit quantization; m=156 training spectra. The highest values of n shown for ICA vectors was the optimum found for each method according to CSCM metric.

ber of ICA vectors had to be used to show dependence upon n for the accuracy of this basis because the reconstructions improve substantially in quality if we use a larger number of ICA vectors, compared with the results obtained with PCA and NMF. In Table 2 we show some numerical results of these simulations. Figure 8 is drawn for $n=9$ ICA basis vectors in all cases, though the shape of the respective optimum sensors is almost the same for every value of n.

The optimum sensors found when using NMF basis vectors are very similar to the ones obtained before for PCA basis vectors for the three spectral estimation methods, as shown in Fig. 8. The accuracy achieved in the spectral reconstructions is also comparable (Table 2). Furthermore, we found that the best results were achieved if three NMF vectors were used with three sensors with the Maloney–Wandell and Imai–Berns methods. Thus we found no practical advantage or disadvantage in using NMF instead of PCA to obtain a linear basis for the spectral recovery of skylight SPDs, except that longer computation time is needed to calculate a NMF basis compared with PCA and that it is compulsory in NMF to choose the number of vectors to be generated before doing it (the shape of the vectors depends on the number to be generated,[9] which does not apply to PCA). Some authors[9,39] maintain that NMF has two advantages over

PCA: First, NMF basis vectors are strictly positive and can be understood as physically realizable additive colors;[9] second, their truncated-positive pseudoinverses[39] could represent the spectral sensitivities of the sensors, the responses of which, ρ, would be directly the weights, ϵ, in the linear combinations in Eq. (3). Nevertheless, the spectral shape of these NMF basis sensors is not so easily achievable as that of Gaussian sensors.

The three optimum sensors obtained with the ICA basis are quite different from those obtained with PCA or NMF bases for the Maloney–Wandell and Imai–Berns methods, while they are very similar for the Shi–Healey method (Fig. 8). The reconstructions using three sensors and ICA vectors are more accurate with all the estimation methods tested than those obtained with PCA or NMF bases, as other authors have also found[39,40] when recovering spectral reflectances of objects or radiance spectra of scenes. For the Maloney–Wandell method with three sensors, the ICA results improve on those of PCA or NMF bases even when using just three vectors, and the ICA results are improved by increasing n up to 12. With the Imai–Berns and Shi–Healey methods, the ICA results are also better than those obtained using PCA or NMF but at the price of using more vectors, where the highest value of n shown for the ICA vectors was the optimum found (Table 2).

D. Speed of Algorithms and Quantization

In this section we make a brief comparison between the time required by each method to estimate the spectra as a function of m (the size of the training set). We presume we have already trained the system; i.e., we have calculated the matrices V, Λ, W, and G described in Section 2 from the training spectra and only have to measure the time required for estimating the spectra from three optimum sensor responses. Hence the Maloney–Wandell, Imai–Berns, and Wiener methods have only to compute a matrix multiplication in the form
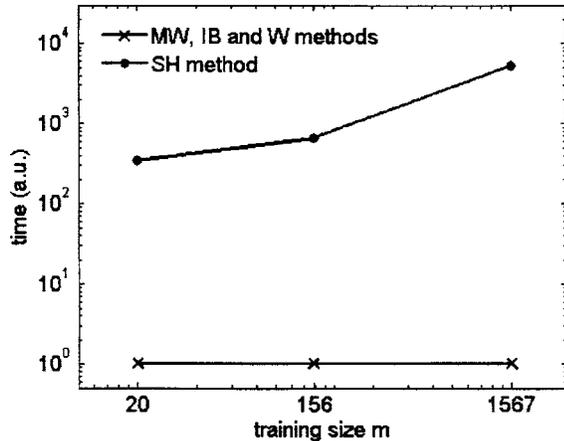

Fig. 9. Relative comparison of the computation time with the four recovery methods as a function of the training-set size m. Three sensors are used with all the methods (MW, Maloney–Wandell[6]; IB, Imai–Berns[15]; SH, Shi–Healey[16]; W, Wiener[18]). Three basis vectors are used with the Maloney–Wandell[6] and Imai–Berns[15] methods, while five basis vectors are used with the Shi–Healey[16] method.

$$E = X\rho, \tag{18}$$

where X is an $N \times 3$ matrix that transforms sensor responses to skylight spectra. This matrix is estimated in different ways depending on the method used. It would not be surprising if these three methods took the same computing time. In Fig. 9 we show a vertical time scale, in arbitrary units, which shows the relative time taken by each method to recover our 1567 skylight spectra using three sensors and different values for m. In this simulation the Maloney–Wandell and Imai–Berns methods were developed using three basis vectors, while the Shi–Healey method used five.

We can see that the Maloney–Wandell, Imai–Berns, and Wiener methods take the same computing time for a given task once the system is trained. The Shi–Healey method, although it gives the best results, is extremely slow compared with the other three methods tested here, especially when m is large. All these parameters should be taken into account in the design of a practical multispectral system. When selecting the most suitable estimation method, one should balance the accuracy hoped for against the computation time needed to achieve the recoveries. In a multispectral system with many pixels and one spectrum per pixel, computation time may be quite considerable if a slow method is used.

To summarize all the results shown in previous sections, we present in Table 3 a brief comparison between the most important characteristics and the results provided by the four spectral estimation methods studied here.

Finally, we compare the effect of using uniform versus nonuniform quantization at various bit levels, although typically the influence of the quantization noise is much less than the influence of other noise sources.[4,17] In Table

Table 3. Differences and Similarities among the Four Spectral Estimation Methods

Method	Maloney-Wandell	Imai-Berns	Shi-Healey	Wiener
Linear basis	Yes	Yes	Yes	No
Training spectra	Yes (PCA)	Yes (PCA and pseudo-inverse)	Yes (PCA and comparison)	Yes (pseudo-inverse)
Spectral sensitivities	Yes	No	Yes	No
Computation time	Fast and constant with m	Fast and constant with m	Slow and increasing with m	Fast and constant with m
Influence of training set on optimum sensors	Low	Low	Low	Low
Influence of training set on results	Low	Low	High	Low
Influence of noise on optimum sensors	Sharpen	Sharpen and displacement	Sharpen	Sharpen
Influence of noise on results	40dB:30dB:26dB CSCM=1:2:3	40dB:30dB:26dB CSCM=1:2:3	40dB:30dB:26dB CSCM=1:2:3	40dB:30dB:26dB CSCM=1:2:3
$n = k$ with PCA	Better $n=k$	Better $n=k$	Better $n= 6, 7$ depending on SNR	--

Table 4. Mean Values±Standard Deviations for Various Metrics When Recovering the Complete Test Set of 1567 Skylight Spectra Using the Optimum Three Sensors Found in Each Case at a SNR of 40 dB and Using $m = 1567$ Training Spectra

Method	Quantization	Bits	GFC	ΔE^{*}_{ab}	CSCM
Maloney-Wandell[a]	uniform	8	0.9993±0.0012	0.8384±0.5619	2.2722±1.1569
		10	0.9994±0.0012	0.8132±0.5567	2.0563±1.1148
		12	0.9994±0.0012	0.8100±0.5652	2.0125±1.0836
	potential $p = 0.33$	8	0.9993±0.0012	0.8182±0.5675	2.1180±1.1056
		10	0.9994±0.0012	0.8110±0.5564	2.0285±1.1068
		12	0.9994±0.0012	0.8106±0.5536	2.0099±1.1029
	μ-law $\mu = 255$	8	0.9994±0.0012	0.8177±0.5746	2.0867±1.1256
		10	0.9994±0.0012	0.8103±0.5576	2.0296±1.1079
		12	0.9994±0.0012	0.8092±0.5635	2.0078±1.1045
Imai-Berns[a]	uniform	8	0.9993±0.0012	0.8286±0.5201	2.2912±1.1649
		10	0.9993±0.0012	0.7924±0.4950	2.0324±1.0955
		12	0.9993±0.0012	0.7725±0.5104	2.0089±1.0866
	potential $p = 0.33$	8	0.9993±0.0012	0.8064±0.5103	2.1320±1.1276
		10	0.9993±0.0012	0.7920±0.4934	2.0144±1.0912
		12	0.9993±0.0012	0.7733±0.4901	2.0075±1.0781
	μ-law $\mu = 255$	8	0.9993±0.0012	0.8034±0.5089	2.1085±1.0936
		10	0.9993±0.0012	0.7928±0.4929	2.0121±1.0913
		12	0.9993±0.0012	0.7733±0.4900	2.0061±1.0782
Shi-Healey[b]	uniform	8	0.9996±0.0003	0.6210±0.4763	1.3552±0.8273
		10	0.9997±0.0003	0.5628±0.4709	1.1676±0.7902
		12	0.9997±0.0003	0.5730±0.4611	1.1727±0.7586
	potential $p = 0.33$	8	0.9997±0.0004	0.6012±0.4875	1.2448±0.8048
		10	0.9997±0.0004	0.5624±0.4826	1.1787±0.8076
		12	0.9997±0.0003	0.5690±0.4808	1.1773±0.7842
	μ-law $\mu = 255$	8	0.9997±0.0003	0.5840±0.4784	1.2187±0.7916
		10	0.9997±0.0003	0.5562±0.4713	1.1569±0.7928
		12	0.9997±0.0003	0.5687±0.4789	1.1666±0.7723
Wiener	uniform	8	0.9993±0.0012	0.8166±0.5020	2.2432±1.1310
		10	0.9994±0.0012	0.7742±0.4968	2.0139±1.0794
		12	0.9994±0.0012	0.7873±0.5240	1.9882±1.0422
	potential $p = 0.33$	8	0.9993±0.0012	0.7945±0.5021	2.0766±1.0897
		10	0.9994±0.0012	0.7721±0.4990	2.007±1.0640
		12	0.9994±0.0012	0.7868±0.4946	1.9816±1.0773
	μ-law $\mu = 255$	8	0.9993±0.0012	0.7972±0.4976	2.0598±1.0893
		10	0.9994±0.0012	0.7728±0.4975	2.0070±1.0626
		12	0.9994±0.0012	0.7872±0.4952	1.9835±1.0767

[a]Three sensors and PCA basis vectors are used.
[b]Three sensors and five PCA basis vectors are used.

4 we show the mean and standard deviation values throughout the complete test set of 1567 skylight spectra (the training-set size, m, was also 1567) when these were recovered using the optimum three sensors found in Section 4 with each method at a SNR of 40 dB. They are A/D converted by using uniform quantization and two different nonlinear transformations of the data prior to quantization; i.e., the potential transformation[28] (we transform each i component of the vector of sensor responses from ρ_i to ρ_i^p, with p being a real number of less than unity) or μ-law transformation,[38] which is a usual quantization strategy used in voice communications in which $\mu = 255$. The intention of these two transformations was to assign more quantum steps whenever the signal was lower, hence increasing the mean quantization SNR (the SNR achieved if only quantization noise was present[38]). It can

be seen in Table 4 that an increase in the number of bits from 8 to 10 results in a significant improvement in the metrics tested, while the results achieved with 12 bits are very similar to those of 10-bit quantization. The two non-uniform quantization schemes are also recommendable if we use only 8 bits, but the improvement achieved with these previous data-compression strategies when quantizing with 10 or 12 bits is negligible.

5. CONCLUSIONS

We have presented a complete study of a practical multispectral system for the spectral recovery of skylight from the noise-affected responses of a set of from three to five Gaussian sensors. We searched for the optimum sensors for this multispectral system by testing four different

spectral estimation methods: the Maloney–Wandell,[6] Imai–Berns,[15] Shi–Healey,[16] and Wiener[18] methods. We found that the position, width, relative height, and number of the optimum sensors are different for each method and that they also depend on the noise present in the system and the characteristics of the linear basis used. With the Maloney–Wandell, Imai–Berns, and Wiener methods, the optimum spectral sensitivities and the accuracy of the reconstructions depended only slightly on the size of the training set of spectra, and thus we could use small training sets of spectra with these methods. For the Shi–Healey method we found that an increase in the size of the training set of spectra provided better results and a small sharpening of the optimum sensors. Spectral sharpening of the optimum sensors was also found with the Maloney–Wandell and Wiener methods when the noise and the number of sensors in the multispectral system increased. Thus we conclude that we should accurately estimate system noise first and then use the set of optimum sensors found for the corresponding noise level.

Our aim was to find the best reconstructions of skylight spectral curves from the responses of the optimum set of Gaussian sensors of a given estimation method, from spectral, colorimetric, and radiometric points of view, even in the presence of noise. We have concluded that the Shi–Healey method proved to be the best method for this task, providing recovered skylight spectral curves very similar to those measured using a spectroradiometer, thus allowing us to use a multispectral system instead. Nevertheless, the accuracy and computation time of the Shi–Healey method depends highly on the training-set size, proving to be extremely slow compared with the Maloney–Wandell, Imai–Berns, and Wiener methods. Our preferred approach would be to use the Wiener estimation method because it is fast and robust to noise, even when using a small training set of spectra. It does not require the previous calculation of either a linear basis or the spectral sensitivities of the system, and finally it affords the best results, apart from those obtained with the Shi–Healey method, while still permitting the construction of a multispectral system with a few Gaussian sensors for accurately estimating spectral skylight.

We found that with the Shi–Healey method an increase in the number of sensors did not necessarily improve the accuracy of the recovered spectra if noise was high because each sensor's individual contribution to noise was more appreciable than the slight improvement achieved in low-noise situations when increasing the number of sensors to more than four. With the other three methods little improvement was achieved when using five sensors instead of four to recover skylight spectra from sensor responses if noise was high.

We searched for the optimum number of PCA basis vectors to be used with the Maloney–Wandell, Imai–Berns, and Shi–Healey methods in each noise situation and found that it was always preferable to use the same number of PCA vectors and sensors with the Maloney–Wandell and Imai–Berns methods. Since the Shi–Healey method is designed to use higher dimensionalities, we found the best results when using seven PCA vectors for low noise and six PCA vectors for higher noise. We also tested the effect on the optimum sensors and accuracy in

the reconstructions for three different schemes for obtaining linear bases, i.e., PCA, NMF, and ICA, and found very similar results with PCA and NMF bases. ICA basis vectors provided better results with all the estimation methods that required linear bases, at the price of using more vectors.

Finally, we studied the effect of uniform and nonuniform quantization noise with different numbers of bits and found a significant improvement when previously compressing the data and using at least 10 bits in the A/D conversion.

ACKNOWLEDGMENTS

REFERENCES

1. R. M. Goody and Y. L. Yung, *Atmospheric Radiation, Theoretical Basis*, 2nd ed. (Oxford U. Press, 1995), Chap. 5.
2. J. Y. Hardeberg, "Acquisition and reproduction of color images: colorimetric and multispectral approaches," Ph.D. dissertation (Ecole Nationale Supérieure des Télécommunications, Paris, 1999), pp. 121–174.
3. N. Metropolis, A. Rosenbluth, M. Rosenbluth, A. Teller, and E. Teller, "Equations of state calculations by fast computing machines," J. Chem. Phys. **21**, 1087–1092 (1953).
4. M. A. López-Álvarez, J. Hernández-Andrés, J. Romero, and R. L. Lee Jr., "Designing a practical system for spectral imaging of skylight," Appl. Opt. **44**, 5688–5695 (2005).
5. M. A. López-Álvarez, J. Hernández-Andrés, E. M. Valero, and J. L. Nieves, "Colorimetric and spectral combined metric for the optimization of multispectral systems," in *Proceedings of the 10th Congress of the International Colour Association (AIC'05)* (AIC, 2005), pp. 1685–1688.
6. L. T. Maloney and B. A. Wandell, "Color constancy: a method for recovering surface spectral reflectance," J. Opt. Soc. Am. A **3**, 29–33 (1986).
7. D. H. Marimont and B. A. Wandell, "Linear models of surface and illuminant spectra," J. Opt. Soc. Am. A **9**, 1905–1913 (1992).
8. J. Romero, A. García-Beltrán, and J. Hernández-Andrés, "Linear bases for representation of natural and artificial illuminants," J. Opt. Soc. Am. A **14**, 1007–1014 (1997).
9. G. Buchsbaum and O. Bloch, "Color categories revealed by non-negative matrix factorization of Munsell color spectra," Vision Res. **42**, 559–563 (2002).
10. P. O. Hoyer, "Non-negative factorization with sparseness constraints," J. Mach. Learn. Res. **5**, 1457–1469 (2004).
11. D. D. Lee and H. S. Seung, "Learning the parts of objects by non-negative matrix factorization," Nature (London) **401**, 788–793 (1999).
12. A. Hyvärinen, J. Karhunen, and E. Oja, *Independent Component Analysis*, 1st ed. (Wiley, 2001), pp. 147–292.
13. T. W. Lee, M. Girolami, and T. J. Sejnowski, "Independent component analysis using an extended infomax algorithm for mixed sub-Gaussian and super-Gaussian sources," Neural Comput. **11**, 417–441 (1999).
14. D. Connah, S. Westland, and M. G. A. Thomson,

"Optimization of a multispectral imaging system," in *Proceedings of the 1st European Conference on Colour Graphics, Image and Vision* (Society for Imaging Science and Technology, 2002), pp. 619–622.

15. F. H. Imai and R. S. Berns, "Spectral estimation using trichromatic digital cameras," in *Proceedings of the International Symposium on Multispectral Imaging and Color Reproduction for Digital Archives* (Society of Multispectral Imaging of Japan, 1999), pp. 42–48.

16. M. Shi and G. Healey, "Using reflectance models for color scanner calibration," J. Opt. Soc. Am. A **19**, 645–656 (2002).

17. H. Haneishi, T. Hasegawa, A. Hosoi, Y. Yokoyama, N. Tsumura, and Y. Miyake, "System design for accurately estimating spectral reflectance of art paintings," Appl. Opt. **39**, 6621–6632 (2000).

18. W. K. Pratt and C. E. Mancill, "Spectral estimation techniques for the spectral calibration of a color image scanner," Appl. Opt. **15**, 73–75 (1976).

19. J. L. Nieves, E. M. Valero, S. M. C. Nascimento, J. Hernández-Andrés, and J. Romero, "Multispectral synthesis of daylight using a commercial digital CCD camera," Appl. Opt. **44**, 5696–5703 (2005).

20. D. C. Day, "Filter selection for spectral estimation using a trichromatic camera," M.Sc. dissertation (Rochester Institute of Technology, 2003), http://www.art-si.org/PDFs/Acquisition/DCDayMSThesis03.pdf.

21. N. Shimano, "Evaluation of a multispectral image acquisition system aimed at reconstruction of spectral reflectances," Opt. Eng. (Bellingham) **44**, 107005 (2005).

22. N. Shimano, "Optimization of spectral sensitivities with Gaussian distribution functions for a color image acquisition device in the presence of noise," Opt. Eng. (Bellingham) **45**, 013201 (2006).

23. N. Shimano, "Suppression of noise effects in color correction by spectral sensitivities of image sensors," Opt. Rev. **9**, 81–88 (2002).

24. M. A. López-Álvarez, J. Hernández-Andrés, J. L. Nieves, and J. Romero, "Influence of the recovery method on the optimum sensors for spectral imaging of skylight," Proc. SPIE **6062**, 6062-9 (2006).

25. V. Cheung, C. Li, S. Westland, J. Y. Hardeberg, and D. R. Connah, "Characterization of trichromatic color cameras by using a new multispectral imaging technique," J. Opt. Soc. Am. A **22**, 1231–1240 (2005).

26. M. Vilaseca, J. Pujol, and M. Arjona, "Illuminant influence on the reconstruction of near-infrared spectra," J. Imaging Sci. Technol. **48**, 111–119 (2003).

27. D. Connah, S. Westland, and M. G. A. Thomson, "Recovering spectral information using digital camera systems," Color Technol. **117**, 309–312 (2001).

28. P. D. Burns and R. S. Berns, "Quantization in multispectral color image acquisition," in *Proceedings of the IS&T 7th Color Imaging Conference: Color Science, Systems and Applications* (Society for Imaging Science and Technology, 1999), pp. 32–35.

29. J. Hernández-Andrés, J. Romero, and R. L. Lee, Jr., "Colorimetric and spectroradiometric characteristics of narrow-field-of-view clear skylight in Granada, Spain," J. Opt. Soc. Am. A **18**, 412–420 (2001).

30. S. M. Sze, *Physics of Semiconductor Devices*, 2nd ed. (Wiley, 1981), pp. 362–510.

31. S. Franco, *Design with Operational Amplifiers and Analog Integrated Circuits*, 3rd ed. (McGraw-Hill, 2002), pp. 311–346.

32. R. A. Yotter and D. M. Wilson, "A review of photodetectors for sensing light-emitting reporters in biological systems," IEEE Sens. J. **3**, pp. 288–303 (2003).

33. P. Alotto, A. Caiti, G. Molinari, and M. Repetto, "A multiquadrics-based algorithm for the acceleration of simulated annealing optimization procedures," IEEE Trans. Magn. **32**, 1198–1201 (1996).

34. F. H. Imai, M. R. Rosen, and R. S. Berns, "Comparative study of metrics for spectral match quality," in *Proceedings of the 1st European Conference on Colour in Graphics, Image and Vision* (Society for Imaging Science and Technology, 2002), pp. 492–496.

35. J. A. S. Viggiano, "Metrics for evaluating spectral matches: a quantitative comparison," in *Proceedings of the 2nd European Conference on Colour Graphics, Imaging and Vision* (Society for Imaging Science and Technology, 2004), pp. 286–291.

36. J. J. Michalsky, "Estimation of continuous solar spectral distributions from discrete filter measurements: II. A demonstration of practicability," Sol. Energy **34**, 439–445 (1985).

37. J. Y. Hardeberg, "Acquisition and reproduction of color images: colorimetric and multispectral approaches," Ph.D. dissertation (Ecole Nationale Supérieure des Télécommunications, Paris, 1999), pp. 134–138.

38. B. P. Lathi, *Modern Digital and Analog Communication Systems*, 2nd ed. (Oxford U. Press, 1989), pp. 132–212.

39. W. Xiong and B. Funt, "Independent component analysis and nonnegative linear model analysis of illuminant and reflectance spectra," in *Proceedings of the 10th Congress of the International Colour Association (AIC'05)* (AIC, 2005), pp. 503–506.

40. E. K. Oxtoby, D. H. Foster, K. Amano, and S. M. C. Nascimento, "How many basis functions are needed to reproduce coloured patterns under illuminant changes?," Perception **31**, Suppl., 66 (2002).